References

[1]*Free Turbulent Shear Flows*, NASA SP-321, 1973.

[2]Launder, B. E., Morse, A. Rodi, W., and Spalding, D. B., "Prediction of Free Shear Flows: A Comparison of the Performance of Six Turbulence Models," *Free Turbulent Shear Flows*, NASA SP-321, 1973, pp. 361-426.

[3]Birch, S. F., and Eggers, J. M., "A Critical Review of the Experimental Data for Developed free Turbulent Shear Layers," *Free Turbulent Shear Flows*, NASA SP-321, 1973, pp. 11-40.

[4]Dash, S. M., Weilerstein, G., and Vaglio-Laurin, R., "Compressibility Effects in Free Turbulent Shear Flows," Air Force Office of Scientific Research, AFOSR-TR-75-1436, Aug. 1975.

[5]Chuech, S. G., Lai, M.-C., and Faeth, G. M., "Structure of Turbulent Sonic Underexpanded Free Jets," *AIAA Journal*, No. 5, Vol. 27, 1989, pp. 549-559.

[6]Sarkar, S., Erlebacher, G., Hussaini, M. Y., and Kreiss, H. O., "The Analysis and Modeling of Dilatational Terms in Compressible Turbulence," *Journal of Fluid Mechanics*, Vol. 227, 1991, pp. 473-493.

[7]Zeman, O., "Dilation Dissipation: The Concept and Application in Modeling Compressible Mixing Layers," *Physics of Fluids A*, Vol. 2, No. 2, 1990, pp. 178-188.

[8]Kim, S. C., "New Mixing-Length Model For Supersonic Shear Layers," *AIAA Journal*, Vol. 28, No. 11, 1990, pp. 1999-2000.

[9]Brescianini, C. P., Morgan, R. G., and Stalker, R. J., "Numerical Modeling of Sidewall Injected Scramjet Experiments in a High Enthalpy Airflow," Shock Tunnel Studies of Scramjet Phenomena — Supplement 6, Dept. of Mechanical Engineering, Univ. of Queensland, Brisbane, Queensland, Australia, 1990.

[10]Bogdanoff, D. W., "Compressibility Effects in Turbulent Shear Layers," *AIAA Journal*, Vol. 21, No. 6, 1983, pp. 926-927.

[11]Papamoschou, D., and Roshko, A., "The Compressible Shear Layer: An Experimental Study," *Journal of Fluid Mechanics*, Vol. 197, 1988, pp. 453-477.

[12]Samimy, M., and Elliott, G. S., "Effects of Compressibility on the Characteristics of Free Shear Layers," *AIAA Journal*, Vol. 28, No. 3, 1990, pp. 439-445.

[13]Rodi, W., "A Review of Experimental Data for Uniform Density Free Turbulent Boundary Layers," *Studies in Convection*, Vol. 1, Academic Press, London, 1975, pp. 79-165.

Taylor Series Approximation of Geometric Shape Variation for the Euler Equations

Arthur C. Taylor III,* Vamshi Mohan Korivi,† and Gene W. Hou‡

Old Dominion University, Norfolk, Virginia 23529

Introduction

THE objective of the present study is the implementation and testing of a linear approximate analysis scheme for the Euler equations, where the treatment of variations in geometric shape is the focus. The method is potentially useful for engineers who must apply modern computational fluid dynamics (CFD) software in a design environment. Detailed documentation of the present work is found in Ref. 1. Approximate analysis is very closely related to a design-oriented discipline known as sensitivity analysis, which involves the calculation of slopes, known as sensitivity derivatives, which are defined as the derivatives of the responses of interest of a particular system with respect to the independent (design) variables of interest.[2-6]

Of particular interest and concern in this research is the use of slopes to predict solution changes in the presence of discontinuities in the flowfield (e.g., shock waves in supersonic flow). Although in the discretization of the governing equations these discontinuities are typically approximated by a continuously differentiable set of algebraic equations, nevertheless, the slopes which are found in a numerical solution in the neighborhood of shocks can fluctuate wildly. Thus a potential difficulty with the technique is identified at the outset, and its effect could vary depending on the particular flowfield and the strength of the discontinuities.

Presentation of Theory

The governing equations considered here are the two-dimensional Euler equations, and are solved in integral conservation law form using a cell-centered finite volume formulation.[7,8] Higher-order accurate upwind discretization of the spatial terms is accomplished using the continuously differentiable flux-vector splitting procedure of van Leer.[9] Numerical integration of the equations in time to steady state is implemented through implicit discretization and "delta" form linearization in time, resulting in the solution at each time step of a large system of linear equations. In essence, steady-state solution of the governing equations is replaced (approximately) by solution of a large system of simultaneous nonlinear algebraic equations over the domain, given as

$$\{R(Q^*)\} = \{0\} \tag{1}$$

where the vector $\{Q^*\}$, the "root," is the steady-state solution for the field variables.

In modern CFD solutions of fluid-flow problems, the geometric shape of the computational domain is defined by the computational mesh, which is generally "body-oriented." A computational mesh is of course defined by the complete set of (x,y) coordinates of the intersection points of the grid lines, and is represented symbolically here as the vector $\{X\}$. Consider a particular fluid-flow problem for which the computational mesh $\{X_1\}$ has been defined, and for which a conventional steady-state solution $\{Q_1^*\}$ is known; that is

$$\{R(Q_1^*, X_1)\} = \{0\} \tag{2}$$

Note in Eq. (2) that the explicit functional dependence of the steady-state discrete algebraic equations on the physical (x,y) coordinates of the mesh is now emphasized. Consider next a second fluid-flow problem, similar to the first except that the geometric shape is different. This defines a second mesh $\{X_2\}$ given by

$$\{R(Q_2^*, X_2)\} = \{0\} \tag{3}$$

A Taylor series expansion about $\{R(Q_1^*, X_1)\}$ is (neglecting higher-order terms)

$$\{R(Q_2^*, X_2)\} = \{R(Q_1^*, X_1)\} + \left[\frac{\partial R(Q_1^*, X_1)}{\partial Q}\right]\{\Delta Q^*\} + \left[\frac{\partial R(Q_1^*, X_1)}{\partial X}\right]\{\Delta X\} \tag{4}$$

where

$$\{\Delta Q^*\} = \{Q_2^*\} - \{Q_1^*\} \quad \text{and} \quad \{\Delta X\} = \{X_2\} - \{X_1\} \tag{5}$$

Since the steady-state solutions satisfy Eqs. (2) and (3), Eq. (4) becomes

$$-\left[\frac{\partial R(Q_1^*, X_1)}{\partial Q}\right]\{\Delta Q^*\} = \left[\frac{\partial R(Q_1^*, X_1)}{\partial X}\right]\{\Delta X\} \tag{6}$$

Received Sept. 20, 1990; revision received July 6, 1991; accepted for publication Dec. 18, 1991.

*Assistant Professor, Department of Mechanical Engineering and Mechanics. Member AIAA.

†Graduate Research Assistant, Department of Mechanical Engineering and Mechanics.

‡Associate Professor, Department of Mechanical Engineering and Mechanics. Member AIAA.

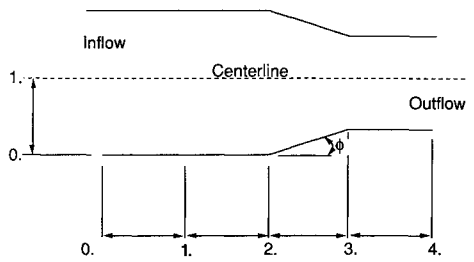

Fig. 1 Subsonic nozzle/supersonic inlet test geometry.

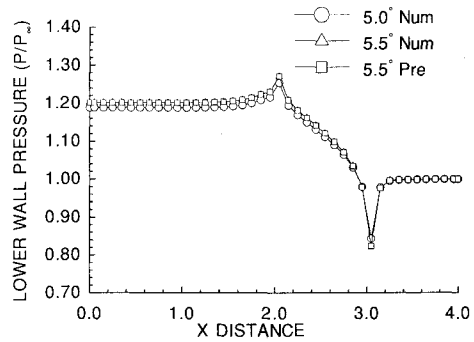

Fig. 2 Subsonic nozzle ($M_\infty = 0.85$, $\phi = 5.5$ deg).

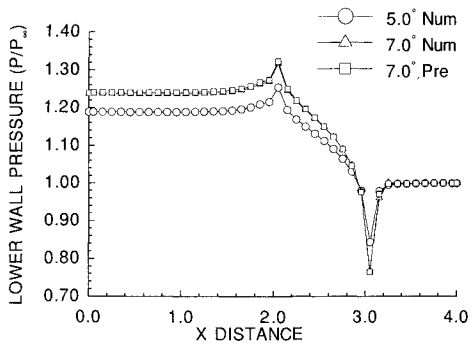

Fig. 3 Subsonic nozzle ($M_\infty = 0.85$, $\phi = 7.0$ deg).

Equation (6) is the central relationship of the basic approximation technique, and understanding it and its potential usefulness is the primary purpose here. When a particular geometric shape variation of interest, $\{X_2\}$, is specified, then $\{\Delta X\}$ and thus the entire right-hand side of Eq. (6) is known. The vector $\{\Delta Q^*\}$, the predicted incremental change in the steady-state solution, is the basic unknown and the solution immediately yields an estimate for $\{Q_2^*\}$. In principle, Eq. (6) can be solved by either 1) direct LU factorization followed by forward and backward substitution, or 2) a number of well-known iterative methods. For a direct solution of Eq. (6), a single LU factorization of the left-hand side coefficient matrix can then be reused for an unlimited number of geometric shape variations, $\{\Delta X\}$. When direct solution of Eq. (6) is not feasible, then an iterative algorithm will be the only recourse, with multiple solutions for multiple geometric shape variations.

The use of Eq. (6) involves two large, sparse, banded Jacobian matrices. On the left-hand side of Eq. (6), the terms of the Jacobian matrix

$$\left[\frac{\partial R(Q_1^*, X_1)}{\partial Q}\right]$$

are well understood and documented, as they are used in CFD codes which employ implicit methods for the numerical time integration of the equations. In addition, Eq. (6) is ideally suited for implementation with an implicit CFD code which uses Newton iteration (i.e., the direct solver algorithm[10] with very large time steps) to determine the known steady-state solution $\{Q_1^*\}$. That is, solutions to Eq. (6) are very rapidly obtained from forward and backward substitution operations using the previously LU factored left-hand side Jacobian matrix already stored in memory at the final Newton iteration for $\{Q_1^*\}$. In typical CFD codes, however, the direct solver approach is not normally used; other more efficient strategies are used instead.

Equation (6) is closely related through the chain rule to a procedure which is used in Refs. 4 and 6 and elsewhere, where sensitivity derivatives are obtained by direct differentiation with respect to the independent (design) variables of interest of the discrete algebraic equations which model the steady-state governing equations [i.e., Eq. (1) in the present study]. In Ref. 2, this connection is discussed in greater detail, with applications to the Euler equations. In this context, it is important to note that the matrix

$$\left[\frac{\partial R(Q_1^*, X_1)}{\partial X}\right]$$

of Eq. (6) is a useful tool in properly accounting for all changes that can be felt throughout the entire domain of a typical body-fitted computational mesh in response to geometric shape changes on the surface of the mesh. A complete description of the construction of this matrix is found in Ref. 1.

All boundary conditions must be consistently linearized in delta form and included in the global Jacobian matrices of *both* sides of Eq. (6) (e.g., the flow tangency boundary condition results in nonzero contributions to both matrices). Although it is common practice to neglect this in implicit time-integration algorithms of typical CFD codes, failure to properly account for the boundary conditions can seriously degrade the quality of the predicted results from the approximation method, as confirmed numerically during preliminary testing of Eq. (6).

Results

The approximate analysis scheme is applied to two test cases, including 1) a family of three similarly shaped fully subsonic nozzles ($M_\infty = 0.85$) and 2) a family of three similarly shaped fully supersonic inlets ($M_\infty = 2.0$). The basic nozzle/inlet shape is illustrated in Fig. 1. Conversion from the subsonic nozzle case to the supersonic inlet case involves only an increase in the freestream Mach number accompanied by appropriate changes to the inflow and outflow boundary conditions. An in-depth description of the test geometry and the boundary conditions is given in Ref. 1.

The ramp angle ϕ of this simple geometry is a single parameter which is varied to generate different (yet closely related) nozzle/inlet shapes. Three ramp angles, 5.0, 5.5, and 7.0 deg were selected, and the 5.0-deg geometry was arbitrarily chosen as the "baseline" geometry. The 5.5-deg geometry thus represents a "small" variation of the 5.0-deg baseline shape, while the 7.0-deg geometry is a significantly larger variation of the baseline geometry. Three computational grids were generated, one for each of these ramp angles, with 41 points in the streamwise direction, and 31 points in the normal direction, uniformly spaced in each direction. Because of symmetry, only the lower half of the domain is gridded.

Machine-zero converged conventional numerical solutions were obtained for the three test geometries, first for the subsonic nozzle case, then for the supersonic inlet case (for a total of six numerical solutions). In the subsonic case, these numerical solutions were generated using the well-known spatially split approximate factorization (AF) time-integration algorithm.[11] In the supersonic case, vertical line Gauss-Seidel (VLGS) relaxation was used.[12]

Using the grid and conventional numerical solutions obtained previously for the 5.0-deg geometry as the baseline, the approximation method [Eq. (6)] was used to generate predicted numerical solutions for the 5.5- and 7.0-deg geometries, first for the subsonic case, and then for the supersonic case (for a total of four predicted numerical solutions). Figures 2–5 illustrate a sample of the numerical results which were produced in these test cases, where in each figure, the static pressure (P/P_∞) is plotted vs distance (x) along the lower wall. Furthermore, in each figure, three solutions are plotted: 1) the 5.0-deg baseline solution (symbolized with circles); 2) a conventional numerical solution of one of the two shape variations, i.e., either the 5.5-deg or the 7.0-deg geometry (symbolized with triangles); and 3) the corresponding predicted numerical solution (symbolized with squares). Thus in each figure the criterion for "success" is squares falling on top of or very close to triangles, which is clearly the case in these figures. More complete numerical results, including comparisons of centerline presures as well as complete pressure contour plots, are provided in Ref. 1.

In generating the predicted numerical results, direct solution of Eq. (6) was employed. In the subsonic cases, a conventional vectorized banded matrix solver was employed which takes advantage of the fact (in terms of both computational work and storage) that outside of the bandwidth, all elements are zero. In the supersonic cases, direct solution of Eq. (6) can be (and is) obtained very efficiently using a single forward sweep of the VLGS algorithm. (See Ref. 7 for full explanation of this.)

A short study was undertaken to evaluate and compare the CPU time requirements for the calculations reported herein, and is fully documented in Ref. 1. In short, this study noted a very large savings in CPU time in generating the estimated numerical solutions using Eq. (6) when compared to the cost of generating complete new conventional CFD solutions of the nonlinear equations. Furthermore, when used as a strategy for generating an improved "initial guess" for subsequent use in obtaining the conventional CFD solutions, the linear approximation strategy produced a net savings in computational cost of about 20% (compared to the cost of simply using the baseline solution as the initial guess). It should not be inferred however that the comparisons of this limited study can be extrapolated to other flow problems.

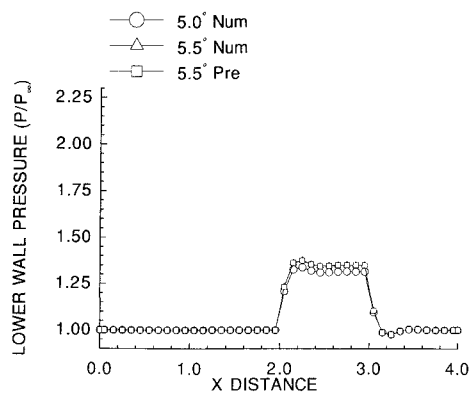

Fig. 4 Supersonic inlet ($M_\infty = 2.0$, $\phi = 5.5$ deg).

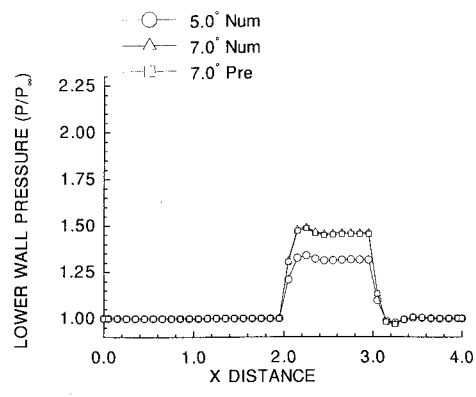

Fig. 5 Supersonic inlet ($M_\infty = 2.0$, $\phi = 7.0$ deg).

Conclusions

This study confirms the possibility of using slopes to accurately predict changes which occur in the field variables of a given flow problem, in response to small changes in geometric shape; and at least for some problems, this is possible even in the presence of discontinuities in the flowfield. Furthermore, the feasibility of applying the principles of sensitivity analysis to calculations involving the Euler equations is (at least in part) confirmed. Although the full potential for gains in computational efficiency through use of the method has not yet been fully assessed, a brief comparative study of CPU times found that the procedure shows promise for saving significant computational work in design oriented CFD applications.

Acknowledgment

This research was supported in part by NSF Grant DMC-865-7917.

References

[1]Taylor, A. C., III, Korivi, V. M., and Hou, G. W., "Sensitivity Analysis Applied to the Euler Equations: A Feasibility Study with Emphasis on Variation of Geometric Shape," AIAA Paper 91-0173, Jan. 1991.

[2]Taylor, A. C., III, Hou, G. W., and Korivi, V. M., "A Methodology For Determining Aerodynamic Sensitivity Derivatives With Respect to Variation of Geometric Shape," *Proceedings of the AIAA/ASME/ASCE/AHS/ASC 32nd Structures, Structural Dynamics and Materials Conference,* AIAA, Washington, DC, 1991 (AIAA Paper 91-1101).

[3]Yates, E. C., Jr., and Desmarais, R., "Boundary Integral Method for Calculating Aerodynamic Sensitivities with Illustration for Lifting Surface Theory," *Proceedings of the International Symposium of Boundary Element Methods (IBEM 89),* Springer-Verlag, New York, 1989.

[4]Elbanna, H. M., and Carlson, L. A., "Determination of Aerodynamic Sensitivity Coefficients in the Transonic and Supersonic Regimes," *Journal of Aircraft,* Vol. 27, No. 6, 1990, pp. 507–518; also AIAA Paper 89-0532, Jan. 1989.

[5]Yates, E. C., Jr., "Aerodynamic Sensitivities from Subsonic, Sonic, and Supersonic Unsteady, Nonplanar Lifting-Surface Theory," NASA TM-100502, Sept. 1987.

[6]Sobieszczanski-Sobieski, J., "The Case For Aerodynamic Sensitivity Analysis," *Sensitivity Analysis in Engineering,* NASA CP-2457, Feb. 1987.

[7]Walters, R. W., and Thomas, J. L., "Advances in Upwind Relaxation Methods," *State of the Art Surveys of Computational Mechanics,* edited by A. K. Noor, American Society of Mechanical Engineers, New York, 1989, pp. 145–183.

[8]Thomas, J. L., van Leer, B., and Walters, R. W., "Implicit Flux-Split Schemes for the Euler Equations," *AIAA Journal,* Vol. 28, No. 6, 1990, pp. 973, 974.

[9]Van Leer, B., "Flux-Vector Splitting for the Euler Equations," Institute for Computer Applications in Science and Engineering, ICASE Rept. 82-30, NASA Langley Research Center, Hampton, VA, Sept. 1982; also *Lecture Notes in Physics,* Vol. 170, 1982, pp. 507–512.

[10]Riggins, D. W., Walters, R. W., and Pelletier, D., "The Use of Direct Solvers for Compressible Flow Computations," AIAA Paper 88-0229, Jan. 1988.

[11]Beam, R. M., and Warming, R. F., "An Implicit Factored Scheme for the Compressible Navier-Stokes Equations," *AIAA Journal,* Vol. 16, No. 4, 1978, pp. 393–402.

[12]Thomas, J. L., and Walters, R. W., "Upwind Relaxation Algorithms for the Navier-Stokes Equations," *AIAA Journal,* Vol. 25, No. 4, 1987, pp. 527–534.